Electronic Supplementary Material (ESI) for Physical Chemistry Chemical Physics.


# Modulating electronic properties and band alignments of arsenene/$MoSi_2N_4$ van der Waals heterostructure via strain and electric field

Jun Zhao†,*, Yunxi Qi†, and Can Yao†

†*New Energy Technology Engineering Laboratory of Jiangsu Province & School of Science, Nanjing University of Posts and Telecommunications, Nanjing, Jiangsu 210023, China*

Hui Zeng*

‡ *School of Microelectronics, Nanjing University of Science and Technology, Nanjing, Jiangsu 210094, China*

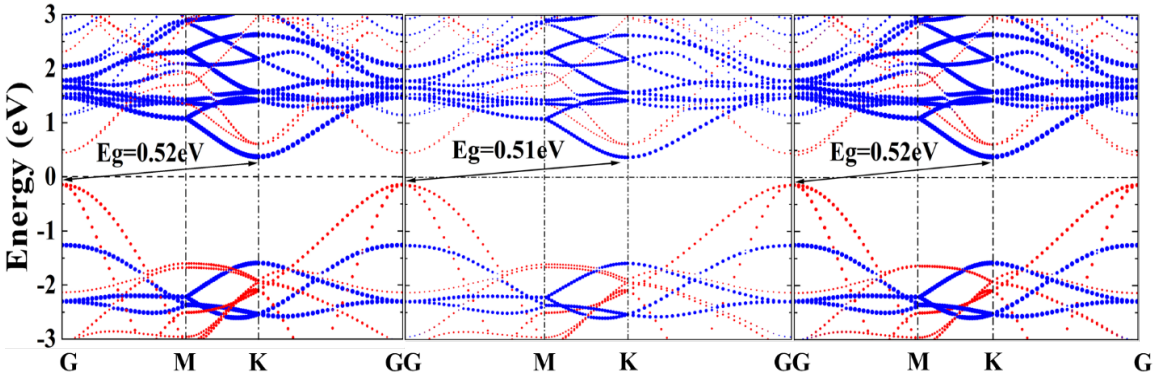


**Fig. S1** The projected electronic structures of the arsenene/$MoSi_2N_4$ heterostructure with $A_1$, $A_2$, and $A_3$ stackings (from left to right). The blue color and red color represent the contributions given by the $MoSi_2N_4$ sublayer and the arsenene sublayer, respectively.

* Authors to whom correspondence should be addressed: zhaojun@njupt.edu.cn (J.Z) and zenghui@njust.edu.cn (H.Z)

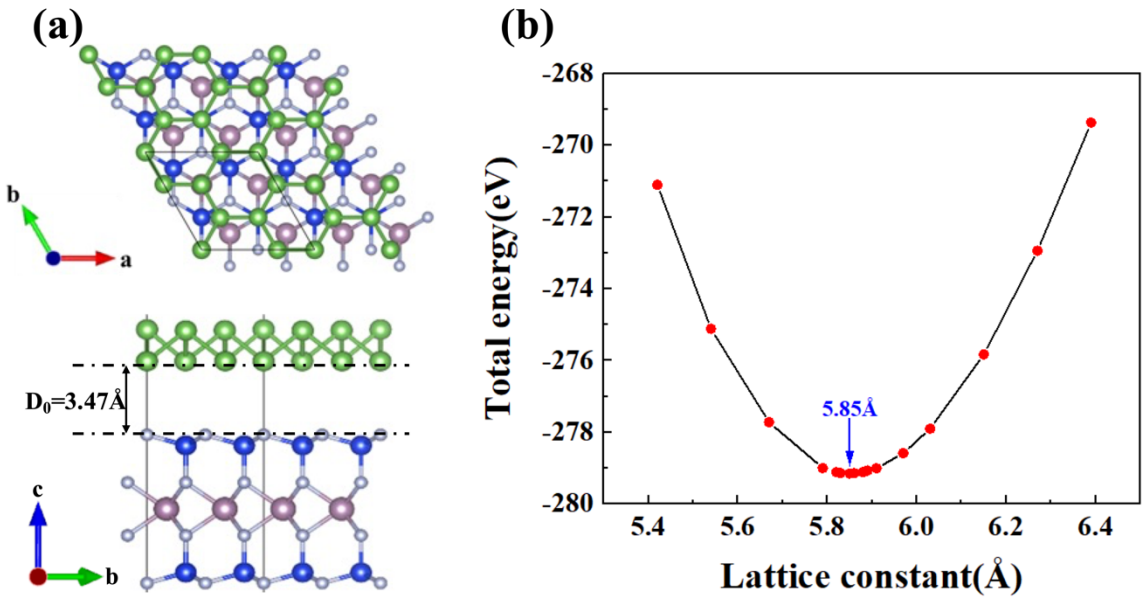


**Fig. S2** The atomic structure of (a) the arsenene/$MoSi_2N_4$ heterostructure with in-plane lattice constant of 5.85 (Å) and (b) the total energy of the heterostructure as a function of different in-plane lattice constants.

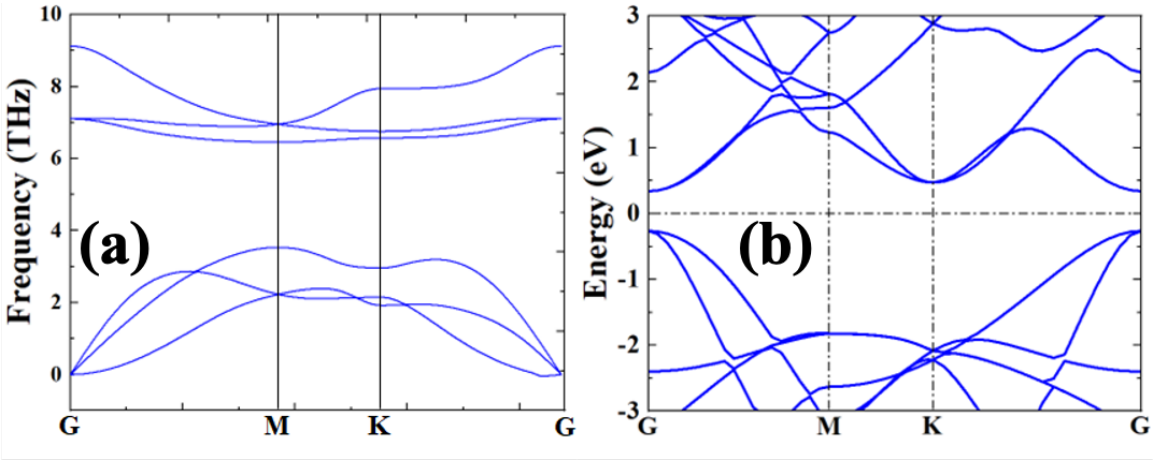


**Fig. S3** The (a) electronic structure and the (b) phonon spectrum of the monolayered arsenene supercell with $\sqrt{3} \times \sqrt{3}$ unit cells and its lattice constants are set to $a$=$b$=5.85 Å.

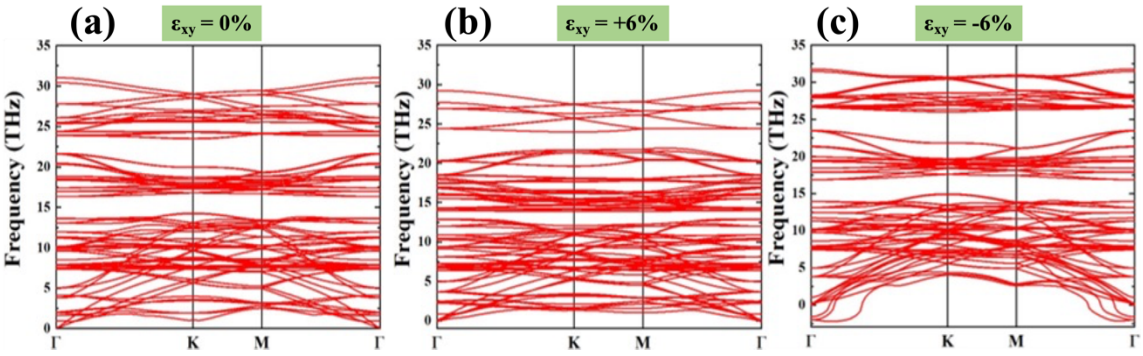


**Fig. S4** Phonon spectral of the arsenene/$MoSi_2N_4$ heterostructure under different in-plane strains when (a) $\varepsilon_{xy}$ = 0%, (b) $\varepsilon_{xy}$ = 6%, and (c) $\varepsilon_{xy}$ = -6%, respectively.

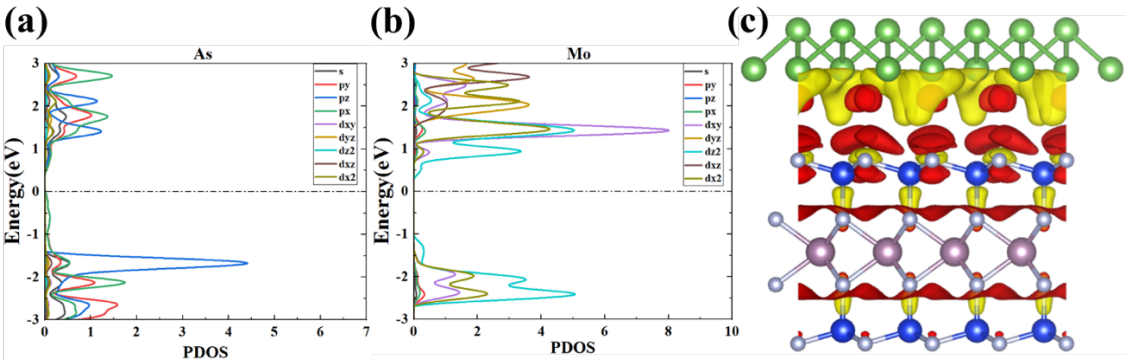


**Fig. S5** Orbital projected density of states (DOS) of the arsenene/$MoSi_2N_4$ heterostructure with all orbitals, including *s*-, *p*-, and *d*-orbitals for (a) As atoms and (b) Mo atoms. (c) The charge density difference of the arsenene/$MoSi_2N_4$ heterostructure with isosurface cutoff of 0.0001 e/Å$^3$, and the electron depletion and accumulation are labelled by red and yellow colors, respectively.

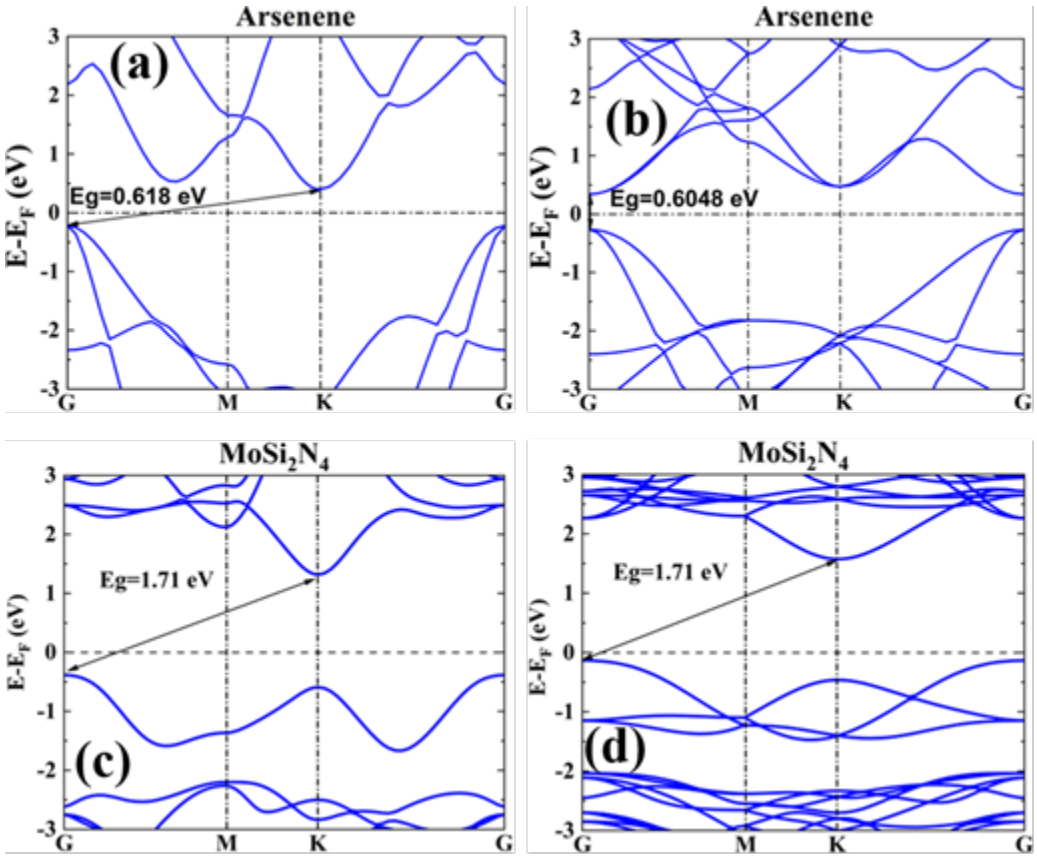


**Fig. S6** The electronic structures of the arsenene monolayer with (a) 1 primitive cell and (b) $\sqrt{3} \times \sqrt{3}$ supercell. The electronic structures of the $MoSi_2N_4$ monolayer with (c) 1 primitive cell and (d) 2×2 supercell.

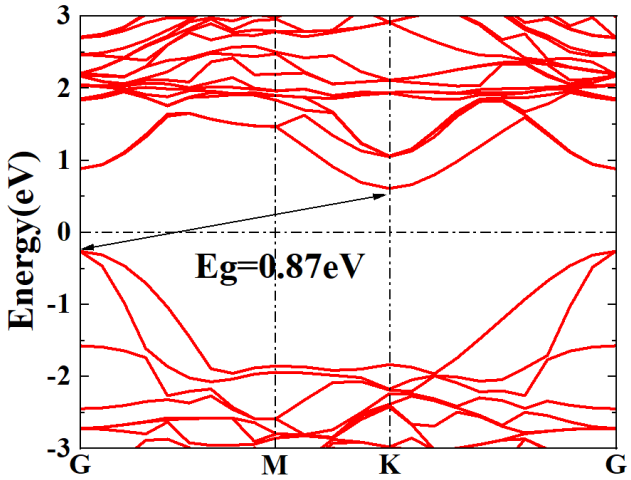


**Fig. S7** HSE06 functional calculation of electronic band structure of the arsenene/$MoSi_2N_4$ heterostructure.

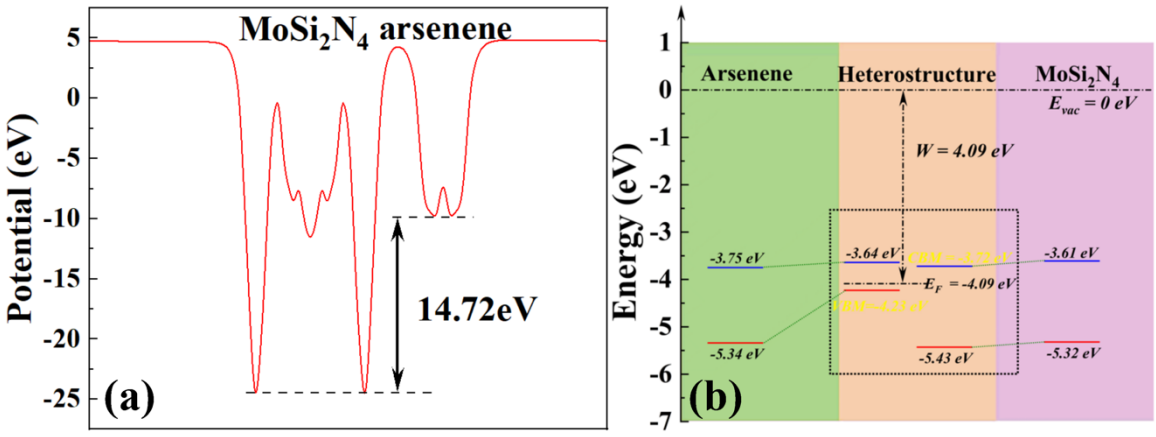


**Fig. S8** The (a) plane-averaged electrostatic potential along z direction and the (b) band edge evolution of the two sublayers and the band edge of the arsenene/$MoSi_2N_4$ heterostructure. The band alignment of the vdW heterostructure is highlighted by black dotted square, and its band edges are denoted by yellow color.

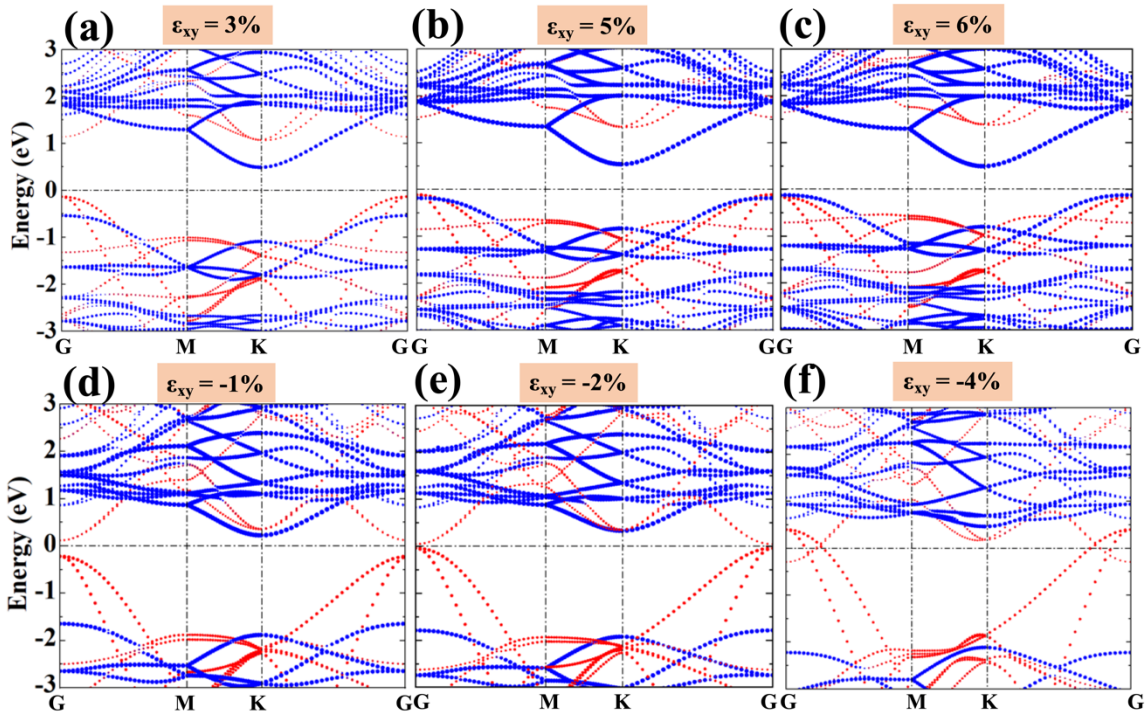


**Fig. S9** The projected band structures of the arsenene/$MoSi_2N_4$ heterostructure under different in-plane biaxial strains. Red color and blue color represent the contributions of the arsenene monolayer and the $MoSi_2N_4$ monolayer, respectively.

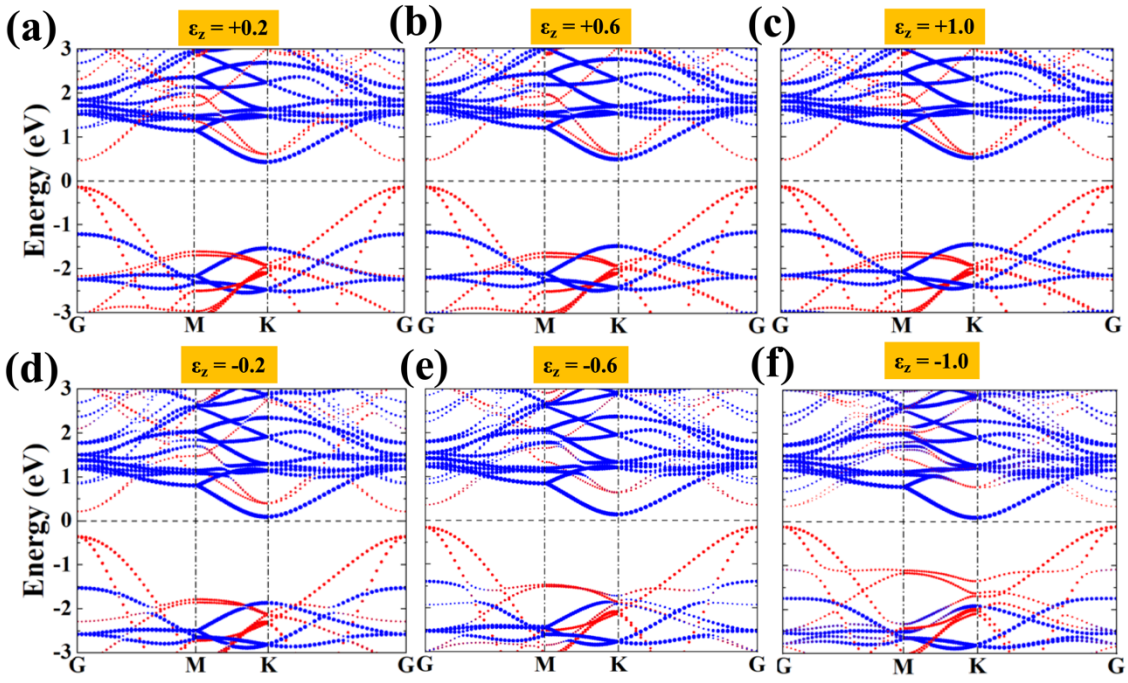


**Fig. S10** The projected band structures of the arsenene/$MoSi_2N_4$ heterostructure under different vertical strains. Red color and blue color represent the contributions of the arsenene monolayer and the $MoSi_2N_4$ monolayer, respectively.

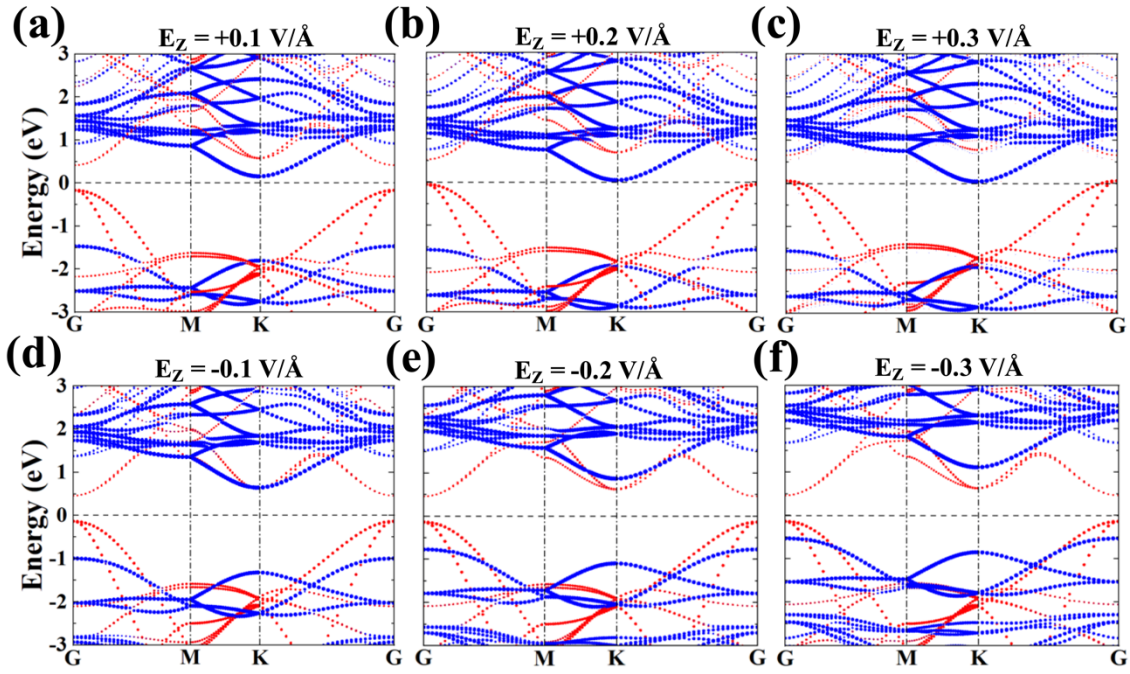


**Fig. S11** The projected band structures of the arsenene/$MoSi_2N_4$ heterostructure under

different external electric fields. Red color and blue color represent the contributions of the arsenene monolayer and the $MoSi_2N_4$ monolayer, respectively.

Table S1 Lattice constants $a$ and $b$, equilibrium distance $D_0$ between the two monolayers, bandgap $E_g$, total energy $E_t$ and binding energy $E_b$ for different stacking structures.

| Stackings | $a = b$ (Å) | $D_0$ (Å) | $E_g$ (eV) | $E_t$ (eV) | $E_b$ (eV) |
|---|---|---|---|---|---|
| $A_1$ | 5.85 | 3.47 | 0.5159 | -279.1501 | -0.5688 |
| $A_2$ | 5.85 | 3.46 | 0.5133 | -279.1496 | -0.5670 |
| $A_3$ | 5.85 | 3.50 | 0.5229 | -279.1489 | -0.5659 |